crystals

MDPI

Article

Polymorphism in *N*-(3-Hydroxyphenyl)-3-methoxybenzamide

Sumaya K. Al-Rawe [1], Daniil Baranov [1], Agnieszka K. Bronowska [1], Celine Cano [2], Michael A. Carroll [1] and Paul G. Waddell [1,*]

[1] School of Natural and Environmental Sciences, Bedson Building, Newcastle University, Newcastle upon Tyne NE1 7RU, UK
[2] Cancer Research UK Newcastle Drug Discovery Unit, Chemistry, School of Natural and Environmental Sciences, Newcastle University, Bedson Building, Newcastle upon Tyne NE1 7RU, UK
* Correspondence: paul.waddell@ncl.ac.uk

Abstract: *N*-(3-hydroxyphenyl)-3-methoxybenzamide was synthesised by amide coupling. After crystallisation, single-crystal X-ray diffraction revealed two distinct polymorphs of the compound: one in the orthorhombic space group $Pna2_1$ with one molecule in the asymmetric unit ($Z' = 1$) and a second in the triclinic space group P-1 with two molecules in the asymmetric unit ($Z' = 2$). A comparison of the structures reveals that the differences between the two can be attributed to conformational variations, disorder, and the dimensionality of the hydrogen bonding networks, with one forming a three-dimensional net and the other forming layers that exhibit approximate $p2_1/b11$ layer group symmetry. Molecular dynamics simulations and well-tempered metadynamics-enhanced sampling calculations provide insight into the transition of one polymorph into the other at room temperature. The efficiency of the crystal packing is assessed by a comparison of the densities and melting points of the two structures.

Keywords: polymorphism; crystal packing; amide coupling; approximate symmetry; *N*-arylbenzamide; molecular dynamics simulations; metadynamics

check for updates

Citation: Al-Rawe, S.K.; Baranov, D.; Bronowska, A.K.; Cano, C.; Carroll, M.A.; Waddell, P.G. Polymorphism in *N*-(3-Hydroxyphenyl)-3-methoxybenzamide. *Crystals* **2024**, *14*, 1070. https://doi.org/10.3390/cryst14121070

Academic Editor: Stefano Carli

Received: 29 November 2024
Revised: 9 December 2024
Accepted: 10 December 2024
Published: 12 December 2024

Copyright: © 2024 by the authors. Licensee MDPI, Basel, Switzerland. This article is an open access article distributed under the terms and conditions of the Creative Commons Attribution (CC BY) license (https://creativecommons.org/licenses/by/4.0/).

1. Introduction

N-Arylbenzamides, a structural motif often associated with biological activity [1–3], may be prepared using a range of methodologies such as amide coupling, metal-catalysed carbonylation, and the reaction of arylisocyanides with styrenes [4–6]. The diversity of synthetic approaches and the corresponding pendant functionality makes this class of drug-like compounds essential constituents of screening libraries. During recent efforts to introduce more examples of this important class of materials into our own compound library, *N*-(3-hydroxyphenyl)-3-methoxybenzamide was synthesised via amide coupling.

N-(3-hydroxyphenyl)-3-methoxybenzamide (Figure 1) had previously been reported by Xu and Alper [7] as having been prepared by palladium-catalysed carbonylation. As only ^{1}H and ^{13}C NMR spectra were reported for this compound, the decision was made to fully characterise it, including by single-crystal X-ray crystallography. The compound was found to crystallise as two polymorphs: polymorph I, which crystallised in the orthorhombic space group $Pna2_1$, and polymorph II, which crystallised in the triclinic space group P-1.

In this work, we detail the structural analysis of the two polymorphs of *N*-(3-hydroxyphenyl)-3-methoxybenzamide with respect to their conformation, intermolecular interactions, and packing efficiency. In addition, the spontaneous transformation of one polymorph to the other was rationalised using molecular dynamics simulations and well-tempered metadynamics-enhanced sampling calculations. This analysis should provide insights into the solid-state properties of *N*-arylbenzamides and add to the sum of our knowledge of polymorphic systems in general [8].

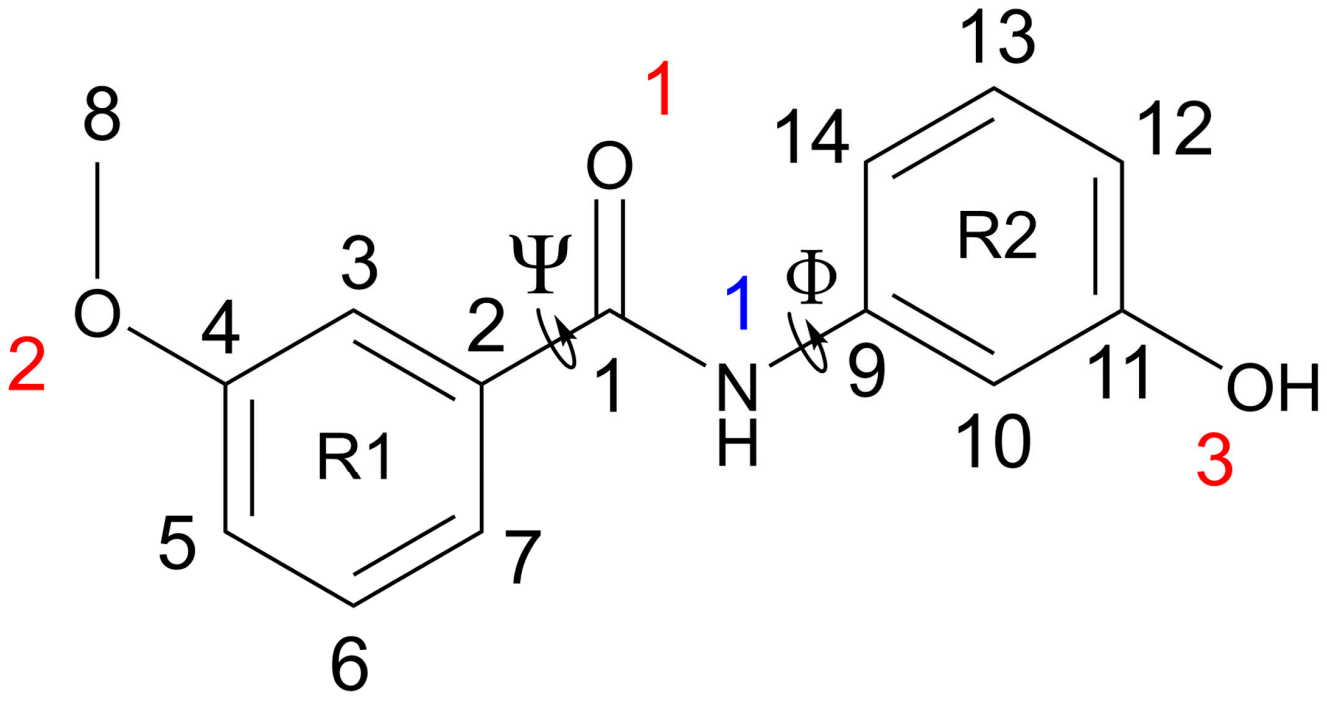


Figure 1. *N*-(3-hydroxyphenyl)-3-methoxybenzamide with the numbering scheme and other labels used in this article.

2. Experimental

2.1. Synthesis

N-(3-hydroxyphenyl)-3-methoxybenzamide: 3-Methoxybenzoic acid (100 mg, 0.66 mmol) was added to a solution of 3-hydroxyaniline (75 mg, 0.69 mmol), HATU (377 mg, 0.99 mmol), and Et_3N (0.23 mL, 1.65 mmol) in DMF (4 mL) and the mixture was stirred for 2 h at 70 °C (Figure 2). The mixture was cooled to room temperature, concentrated in vacuo, using heptane for the azeotropic removal of the DMF. EtOAc (20 mL) was added, and the resulting solution was washed with brine (20 mL). The organic layer was separated, dried (MgSO4), and concentrated in vacuo, to give the crude product, which was purified using column chromatography (SiO_2, 2:1 petrol/EtOAc), yielding the desired amide as a white crystalline solid (100 mg, 0.66 mmol, 62%). R_f = 0.27 (SiO_2, 2:1 petrol: EtOAc); IR ν_{max} (neat) 3380, 3100, 3000, 2850, 2800, 1650, 1580, 1410 cm^{-1}; δ_H (400 MHz; DMSO-d_6) ppm 10.09 (1H, s, NH), 9.42 (1H, s, OH), 7.52 (1H, d, H7, *J* 8 Hz), 7.47 (1H, s, H3), 7.43 (1H, t, H6, *J* 8 Hz), 7.36 (1H, s, H10), 7.19–7.09 (3H, m, H5/H13/H14), 6.52 (1H, d, H12, *J* 8 Hz), 3.84 (3H, s, OMe); δ_C (101 MHz, DMSO-d_6) ppm 165.7 (C1), 159.6 (C4), 158.0 (C11), 140.6 (C9), 137.0 (C2), 130.0 (C6), 129.7 (C13), 120.3 (C7), 117.7 (C5), 113.4 (C3), 111.7 (C14), 111.3 (C12), 108.0 (C10), 55.8 (C8); *m/z* (ESI+) 244(11%, $M+H^+$), 226(23), 135(100), 107(65), Found: $M+H^+$, 244.0966. $C_{14}H_{14}NO_3$ requires 244.0968. Anal calcd for $C_{14}H_{13}NO_3$: C, 69.12; H, 5.39; N, 5.76. Found; C, 69.27; H, 5.37; N, 5.65.

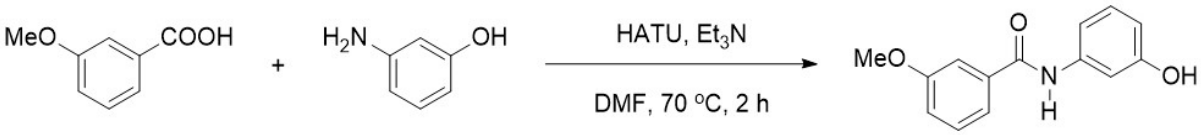


Figure 2. Reaction scheme detailing the amide coupling resulting in *N*-(3-hydroxyphenyl)-3-methoxybenzamide.

2.2. X-Ray Crystallography

Crystals suitable for single-crystal X-ray diffraction were grown by slow evaporation of the solvent from a solution of the compound in petrol–ethylacetate, as was the case

of polymorph I and methanol in the case of polymorph II. The melting point range was 398–400 K for crystals of polymorph I and 381–383 K for crystals of polymorph II.

Single-crystal diffraction data were collected on an XtaLAB Synergy HyPix-Arc 100 diffractometer using copper radiation ($\lambda_{CuK\alpha}$ = 1.54184 Å) at 150 K using an Oxford Cryosystems CryostreamPlus open-flow N_2 cooling device.

Intensities were corrected for absorption using a multifaceted crystal model created by indexing the faces of the crystal for which data were collected [9]. Cell refinement, data collection, and data reduction were undertaken via the software CrysAlisPro [10].

All structures were solved using XT [11] and refined by XL [12] using the Olex2 interface [13]. All non-hydrogen atoms were refined anisotropically, and hydrogen atoms were positioned with idealised geometry, with the exception of those bound to heteroatoms, the positions of which were located using peaks in the Fourier difference map. The displacement parameters of the hydrogen atoms were constrained using a riding model with $U_{(H)}$ set to be an appropriate multiple of the U_{eq} value of the parent atom.

2.3. Molecular Dynamics Simulations

All-atom MD simulations were performed using GROMACS [14] with AMBER99SB-ILDN [15–17] parameters. First, topology files for the crystal structures of polymorph I and polymorph II were generated using the AnteChamber Python Parser Interface (ACPYPE) [18]. Each crystal structure was then positioned in a 3D-PBC cubic box 0.5 nm away from the edge of the protein with TIP3P water [19]. Each polymorph system was subjected to energy minimisation via the steepest descent method for 1000 cycles, with an energy step size of 0.01 nm and a maximum number of steps of 50,000. The maximum force was set at 1000 kJ/mol/nm. Long-range electrostatic interactions were treated using the Particle-Mesh Ewald (PME) method [20], where a cut-off of 1.0 nm for short-range electrostatic and van der Waals interactions was applied.

Following energy minimisation, both systems were subjected to 500 ps NVT and NPT equilibration with a step size of 2 fs. For NVT equilibration, the crystal and water groups were gradually heated to 300 K under the influence of the V-rescale thermostat [21] with a time constant of 0.1 ps. All heavy atom hydrogen bonds were constrained using LINCS (Linear Constraint Solver) position restraints [22]. The non-bonded short-range interactions were treated with the Verlet cut-off scheme, with the cut-off distance set to 1.0 nm. For long-range electrostatics, the PME method was applied, as mentioned above.

For the NPT equilibration, the temperature was kept at 300 K using the same temperature coupler, followed by Parrinello–Rahman pressure coupling [23] with the target pressure of 1 bar. Finally, both polymorphs were subjected to 100 ns simulations to obtain trajectories for subsequent analysis using GROMACS tools. The local flexibility of each crystal, as well as their individual molecules, was assessed via per-atom root mean square fluctuation (RMSF). The variations in dihedral angles throughout the simulation were also assessed.

2.4. Metadynamics

To explore the ϕ and Ψ torsion angles (Figure 1) for the molecules of polymorphs I and II, Plumed 2.90 [24] was used to implement well-tempered metadynamics simulations. For each torsion angle, four atoms were selected to define the dihedral angle of interest. The initial height of each Gaussian potential (HEIGHT) was set to 1.2 kJ/mol, with a width (SIGMA) of 0.05 radians, and a Gaussian added every 1000 simulation steps (PACE). A bias factor (BIASFACTOR) of 10 was also applied. The Gaussian potentials added as a function of the collective variable were recorded in the HILLS file. Subsequently, the Free Energy Surface (FES) was reconstructed by integrating the HILLS data, providing insights into the differences in the energy landscapes for the individual units of polymorphs I and II.

3. Results and Discussion

The two polymorphs of *N*-(3-hydroxyphenyl)-3-methoxybenzamide (Table 1) are similar in terms of their unit cell dimensions and volumes, but a cursory glance at the asymmetric units of the two structures reveals the first salient difference between them. In polymorph I, the asymmetric unit comprises a single molecule, whereas that of polymorph II is made up of two molecules (Figure 3). Interestingly, as polymorph I crystallises in a non-centrosymmetric space group ($Pna2_1$), and polymorph II crystallises in a centrosymmetric space group (P-1), this is contrary to expectation as Z' for the non-centrosymmetric structure is often a multiple of that of the centrosymmetric structure [25], though examples that contradict this observation are known [26].

Table 1. Crystal data and structural refinement details for *N*-(3-hydroxyphenyl)-3-methoxybenzamide.

	Polymorph I	**Polymorph II**
Empirical formula	$C_{14}H_{13}NO_3$	$C_{14}H_{13}NO_3$
Formula weight	243.25	243.25
Temperature/K	150.0(2)	150.0(2)
Crystal system	Orthorhombic	Triclinic
Space group	$Pna2_1$	P-1
a/Å	8.73890(10)	9.0055(4)
b/Å	12.1817(2)	11.8889(5)
c/Å	11.6805(2)	12.4615(3)
α/°	90	75.317(3)
β/°	90	73.306(3)
γ/°	90	71.143(4)
Volume/Å^3	1243.44(3)	1190.23(9)
Z	4	4
ρ_{calc}g/cm^3	1.299	1.357
μ/mm^{-1}	0.757	0.790
F(000)	512.0	512.0
Crystal size/mm^3	0.14 × 0.12 × 0.10	0.19 × 0.10 × 0.03
Radiation	CuKα (λ = 1.54184)	CuKα (λ = 1.54184)
2Θ range for data collection/°	10.492 to 154.536	7.526 to 154.482
Index ranges	$-10 \leq h \leq 10$, $-14 \leq k \leq 14$, $-13 \leq l \leq 14$	$-11 \leq h \leq 11$, $-12 \leq k \leq 14$, $-14 \leq l \leq 15$
Reflections collected	11,271	22,322
Independent reflections	2328 [R_{int} = 0.0349, R_{sigma} = 0.0237]	4748 [R_{int} = 0.0286, R_{sigma} = 0.0234]
Data/restraints/parameters	2328/1/171	4748/532/403
Goodness-of-fit on F^2	1.033	1.043
Final R indexes [I ≥ 2σ (I)]	R_1 = 0.0275, wR_2 = 0.0712	R_1 = 0.0395, wR_2 = 0.1020
Final R indexes [all data]	R_1 = 0.0281, wR_2 = 0.0718	R_1 = 0.0456, wR_2 = 0.1068
Largest diff. peak/hole/e Å^{-3}	0.17/−0.14	0.35/−0.27
Flack parameter	−0.19(11)	n/a

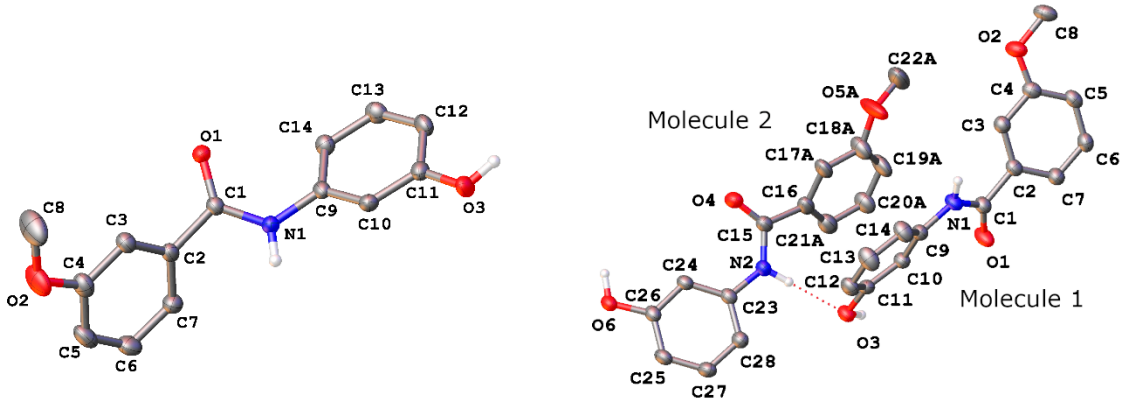


Figure 3. The asymmetric units of polymorph I (**left**) and polymorph II (**right**) with ellipsoids drawn at the 50% probability level. Hydrogen atoms not involved in hydrogen bonding and the minor disorder component in polymorph II was omitted for clarity.

As the term asymmetric unit might suggest, the two molecules representative of the structure of polymorph II are not related by crystallographic symmetry, and this can be attributed to the difference in conformation between them. The conformational variation can be visualised by overlaying the two molecules (Figure 4).

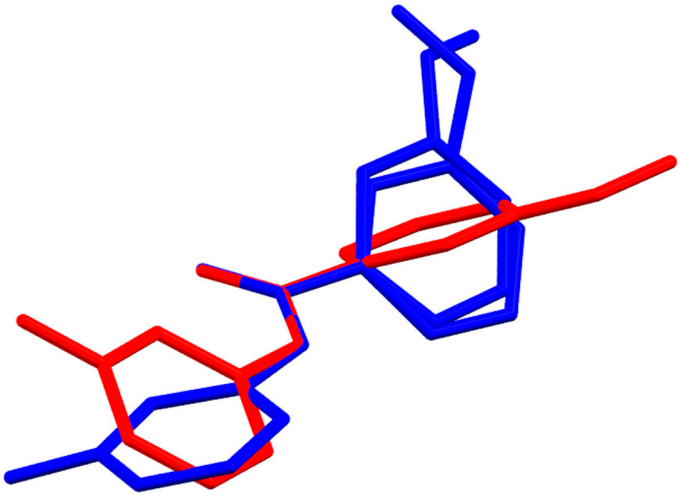


Figure 4. Overlay diagram of molecule 1 (red) and molecule 2 (blue) of polymorph II.

Considering this diagram of the two molecules where the amide groups are overlayed, it becomes apparent that the angles of both benzene rings with respect to the amide are at the root of the difference in conformation together with the orientation of the methoxy substituent. In addition, the methoxyphenyl group of molecule 2 is also observed to be disordered in two positions, principally due to the libration of the benzene ring and the orientation of the methoxy group.

A further overlay diagram can be used to show the conformational variation between the two polymorphs (Figure 5). When compared to those of polymorph II, the single molecule comprising the asymmetric unit of polymorph I can be seen to be most similar to molecule 1; however, the relative positions of both the hydroxyl and methoxy substituents on the benzene rings with respect to the amide group are reversed.

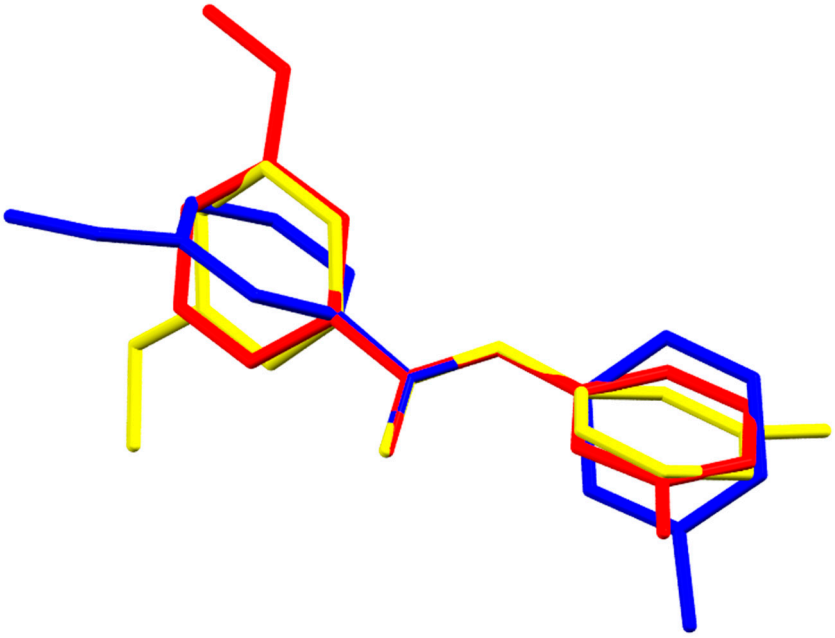


Figure 5. Overlay diagram of polymorph I (yellow) with molecule 1 (red) and molecule 2 (blue) of polymorph II. The minor disorder component was omitted for clarity.

This conformational variation and the different number of molecules in the asymmetric unit have a direct influence on the supramolecular structure of the two polymorphs. As hydrogen bonds manifest in both structures (Table 2), the crystal packing can be characterised using Margaret Etter's graph set notation for hydrogen bonding networks [27].

Table 2. Hydrogen bond distances and angles for *N*-(3-hydroxyphenyl)-3-methoxybenzamide.

	H-A/Å	**D-A/Å**	**D-H···A/°**
	Polymorph I		
O3-H3···O1 [1]	1.86(3)	2.728(2)	170(3)
N1-H1···O1 [2]	2.13(3)	2.965(2)	167(2)
	Polymorph II		
O3-H3···O1 [3]	1.721(18)	2.6405(14)	171.9(15)
O6-H6···O4 [4]	1.759(19)	2.6627(14)	177.6(16)
N1-H1···O6 [5]	2.238(17)	3.0845(15)	163.0(14)
N2-H2···O3	2.016(18)	2.8731(15)	164.4(15)
C13-H13···Mol. 1($R1_{centroid}$) [4]	2.8810(7)	3.593(2)	132.62(9)
C28-H28···Mol. 1($R2_{centroid}$) [5]	3.4542(6)	4.2202(13)	139.31(9)

[1] 3/2 − X, 1/2 + Y, 1/2 + Z; [2] −1/2 + X, 1/2 − Y, +Z; [3] 1 − X, 1 − Y, −Z; [4] 2 − X, −Y, 1 − Z; [5] − 1 + X, 1 + Y, +Z.

The hydrogen bonding network in the structure of polymorph I is a three-dimensional net with hydrogen bonds propagating in three directions. In the crystallographic [100] direction, the amide proton of one molecule donates to the carbonyl oxygen atom of the amide group of a neighbouring molecule, forming a hydrogen-bonded chain with the graph set C(4) (Figure 6). Each molecule in the chain is related to the next molecule by the symmetry of the *a* glide plane.

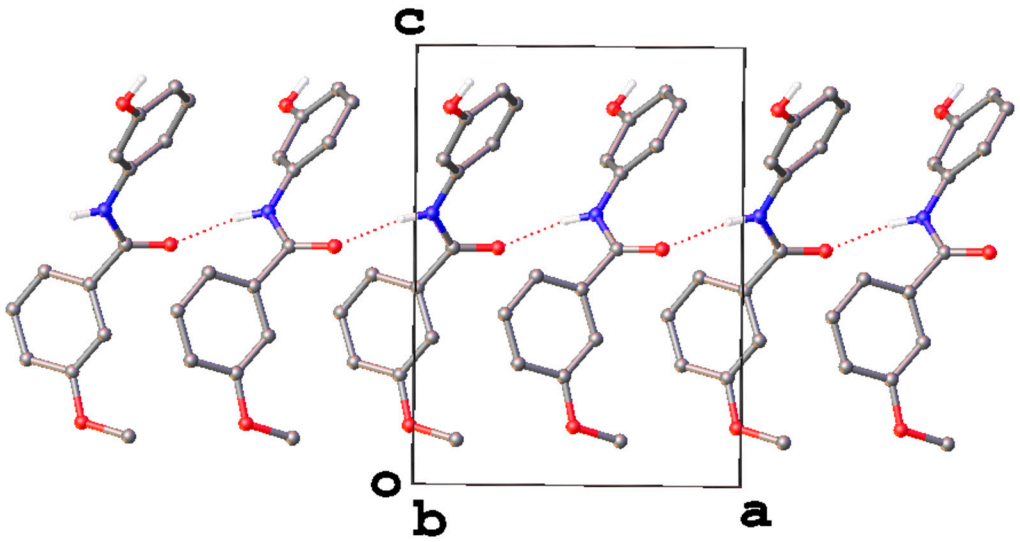


Figure 6. The C(4) hydrogen bonding motif along the [100] direction in the structure of polymorph I viewed down the [010] direction with hydrogen bonds depicted as dashed lines. Hydrogen atoms not involved in hydrogen bonding were omitted for clarity.

Hydrogen bonds where the hydroxyl group acts as a donor to the carbonyl oxygen atom on an adjacent molecule are also observed in the supramolecular structure. These interactions form additional chains with the graph set C(8). As the orientation of each successive molecule in the C(4) chain propagating through the amide groups alternates with the *a* glide plane, two such C(8) chains are observed in both the [011] and [0-11] directions (Figure 7).

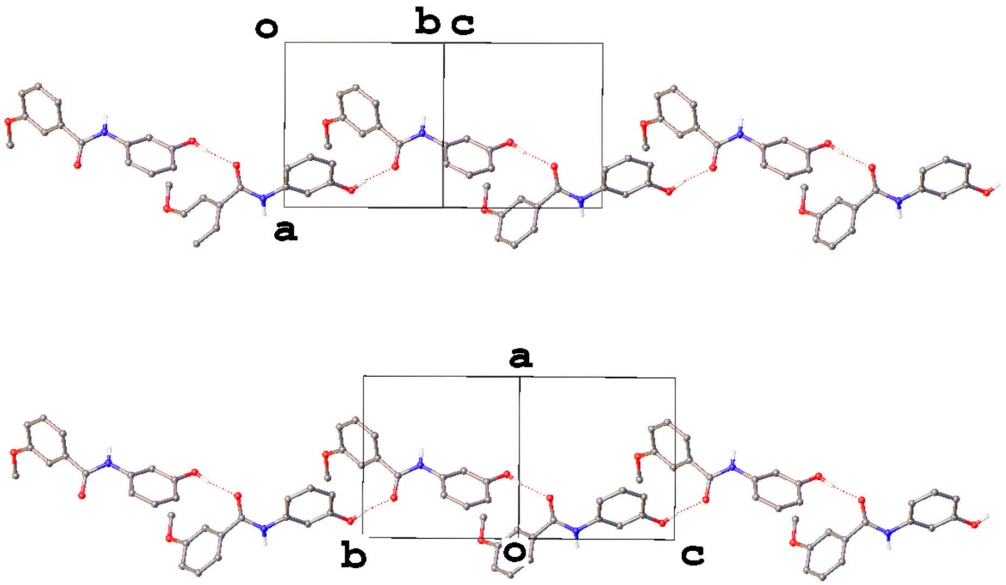


Figure 7. The two C(8) hydrogen bonding motifs along the [011] (**top**) and [0-11] (**bottom**) directions in the structure of polymorph I with hydrogen bonds depicted as dashed lines. Hydrogen atoms not involved in hydrogen bonding were omitted for clarity.

In this case, each molecule in the C(8) chain is related to the next molecule by the symmetry of an *n* glide plane in the appropriate direction. Together, these three chains form a complete, three-dimensional hydrogen-bonded network.

By way of contrast, the hydrogen-bonded network in the structure of polymorph II forms two-dimensional layers of hydrogen-bonded molecules coplanar with the crystallo-

graphic (110) plane. These layers are best described as parallel chains of hydrogen-bonded molecules linked by rings of hydrogen bonds.

The one-dimensional chains form as a result of the amide proton of one molecule donating a hydrogen bond to the hydroxyl group of its neighbour and not the carbonyl group, as was observed for polymorph I. This results in a C(6) chain motif propagating in the [1-10] direction (Figure 8). The chain comprises both molecules 1 and 2, and each pair of these molecules is related to the next pair of molecules by pure translation symmetry.

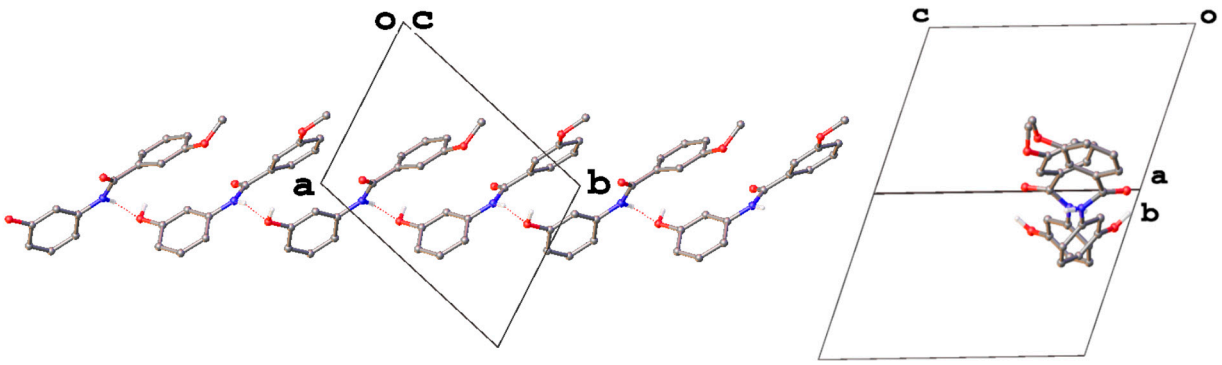


Figure 8. The C(6) hydrogen bonding motif along the [0-11] direction in the structure of polymorph II viewed down the [001] direction (**left**) and down the [0-11] direction showing the approximate glide symmetry (**right**). Hydrogen bonds are depicted as dashed lines, and hydrogen atoms not involved in hydrogen bonding were omitted for clarity.

Though molecules 1 and 2 are not related by crystallographic symmetry, viewing the structure along this direction reveals approximate glide symmetry, which is a clear indication that the structure exhibits approximate symmetry, a feature common in structures with $Z' > 1$ [28–30].

The full nature of this approximate symmetry is revealed by an analysis of the complete two-dimensional hydrogen bonding network (Figure 9). Layers of hydrogen-bonded molecules are formed in the (110) plane due to the linking of the C(6) chains by a hydrogen-bonded $R^2_2(16)$ ring motif comprising two hydrogen bonds, where the hydroxyl group of molecule 1 donates to the carbonyl oxygen atom of an adjacent molecule 1. The two molecules in the ring are related by inversion symmetry so that, by extension, each chain that is linked is related to its neighbour by inversion. It is also worth noting that within the layers, there appear to be weak $\pi\cdots\pi$ interactions with centroid–centroid distances of ca. 4 Å [31] between the R1 and R2 benzene rings of both independent molecules. Interactions of this type were absent from the structure of polymorph I.

In terms of symmetry, as well as the approximate glide symmetry in the [0-11] direction, there is also an approximate 2_1-screw axis symmetry in the [001] direction at an angle of 88°. When taken together, the layers in this structure mimic $p2_1/b11$ layer group symmetry. Interestingly, the approximate symmetry is even more clear if the methoxy groups are ignored. Alternatively, if the R1 ring of either molecule was rotated by 180°, the screw and glide symmetry would also be improved. It would seem that this symmetry is broken to reduce steric interactions between the hydrogen-bonded chains in the [0-11] direction. This results in the methoxy groups superimposing in the direction of the chain with similar z-coordinate values and a somewhat uneven spacing to accommodate them in the structure. What is clear is that, although the orientation of the methoxy groups breaks the symmetry in the layer, the symmetric relationships between most of the atoms appear to have been maintained as much as possible.

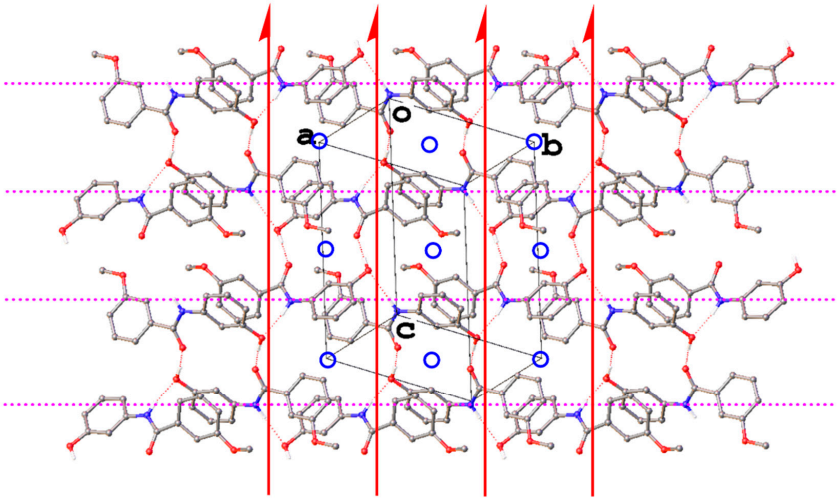


Figure 9. The two-dimensional hydrogen bonding motif in the (110) plane of the structure of polymorph II. The inversion centres (blue circles) and approximate screw axes (red arrows), and glide planes (pink dashes) are shown to demonstrate the approximate $p2_1/b11$ layer group symmetry. Hydrogen bonds are depicted as dashed lines, and hydrogen atoms not involved in hydrogen bonding were omitted for clarity.

The approximate symmetry is confined to the two-dimensional layer, and each layer is offset by ca. 2.80 Å. Between the layers, the most obvious interactions appear to be edge-to-face H···π contact (Table 2).

As might be expected, the dimensionality of the hydrogen bonding networks is apparent in the habits adopted by the crystals of the two polymorphs (Figure 10). Reflecting the three-dimensional nature of the network in polymorph I, the crystals grow as blocks, whereas those of polymorph II are plate-like in nature, indicative of its layered structure.

The differences in the conformation, packing and intermolecular interactions detailed here provide insight into the melting point analyses performed on crystals of both polymorphs. Polymorph I melts at a higher temperature than polymorph II. It stands to reason that this might be the case in polymorph I, as the three-dimensional hydrogen bonding network observed in polymorph I suggests that the crystal is held together by strong interactions in all directions.

The same cannot be said about polymorph II, and its lower melting point can be rationalised by the structural features outlined in this analysis. The higher density of polymorph II attests to the packing efficiency afforded by the π interactions in this structure, but as they are inherently weaker than hydrogen bonds; this, coupled with the lower dimensionality of the two-dimensional hydrogen bonding network in the structure, the weak inter-layer π interactions and the disorder of the methoxy-substituted benzene ring all suggest a structure that is not strongly held together. In addition, crystal structures with $Z' > 1$ are often identified as being metastable [32], and this could well be the case for polymorph II on the basis of the physical and structural evidence.

Indeed, a polymorphic transition was observed and confirmed by melting point measurements. Crystalline samples of polymorph II convert to polymorph I over a short period of time (<3 days at −20 °C), and this would seem to support the argument that polymorph II is metastable. To further investigate the relationship between the two forms and the observed polymorphic transition, equilibrium molecular dynamics (MD) simulations of both polymorphs in explicit water and at room temperature were carried out.

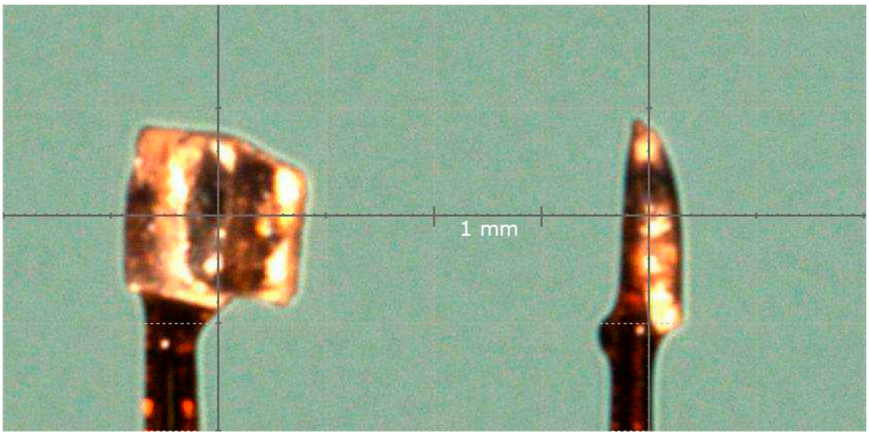


Figure 10. The crystals of polymorph I (**left**) and polymorph II (**right**) for which data were collected.

Analysis of the dihedral angles ϕ and Ψ in the simulation indicates that polymorph I is stable, with the R1 ring controlled by the dihedral angle Ψ observed to 'flip' (Figure 11). The ensemble observed for polymorph II was more diverse; for molecules in the interior of the crystal, rotation of the R1 ring was restricted, while some showed the "flipping" of Ψ or ϕ, destabilising the π···π interactions observed exclusively in polymorph II (Figure 12). In solvent-exposed regions of the crystal, the spontaneous transition to a conformation resembling polymorph I was observed.

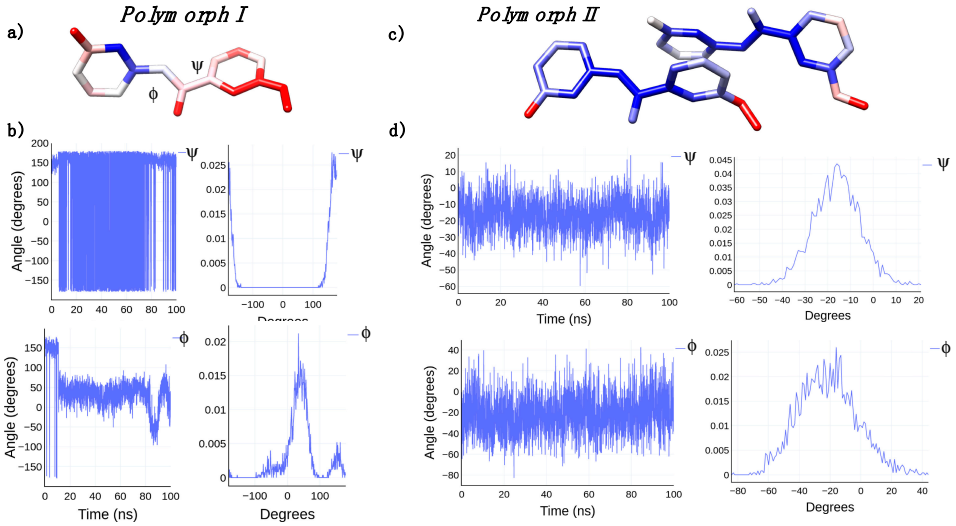


Figure 11. (**a**) The asymmetric unit of polymorph I, coloured to reflect computed root-mean-square fluctuations (RMSFs) from the lowest (blue) to the highest (red) flexibility. Torsional angles ψ and ϕ are highlighted. (**b**) Sampling over torsional angles Ψ and ϕ over 100 ns of equilibrium MD simulations and the torsional distribution of Ψ and ϕ angles for polymorph I. (**c**) The asymmetric unit of polymorph II, coloured as in panel (**a**). (**d**) Sampling over torsional angles Ψ and ϕ for over 100 ns of equilibrium MD simulations and the torsional distribution of Ψ and ϕ angles for polymorph II in the interior of the crystal.

Overall, the simulations explain the decreased stability of polymorph II and suggest that the transition from polymorph II to polymorph I may occur spontaneously. This was further validated through well-tempered metadynamics simulations (Figure 13). The conformation resembling that observed in polymorph I is close to the energy minimum, with other conformations observed in the MD simulation populating the adjacent minima. For polymorph II, the energy minima corresponding to the ϕ and Ψ values observed in the crystal are shallower compared to the minima of polymorph I with a difference of

+4 kJmol^{-1}. The energy barriers calculated are not very high (+8 kJmol^{-1}), indicating that the spontaneous transition from polymorph II to polymorph I is possible, which is consistent with equilibrium MD simulations. The simulations provide a possible confirmation of the metastable nature of polymorph II and the transition from polymorph I to polymorph II at room temperature.

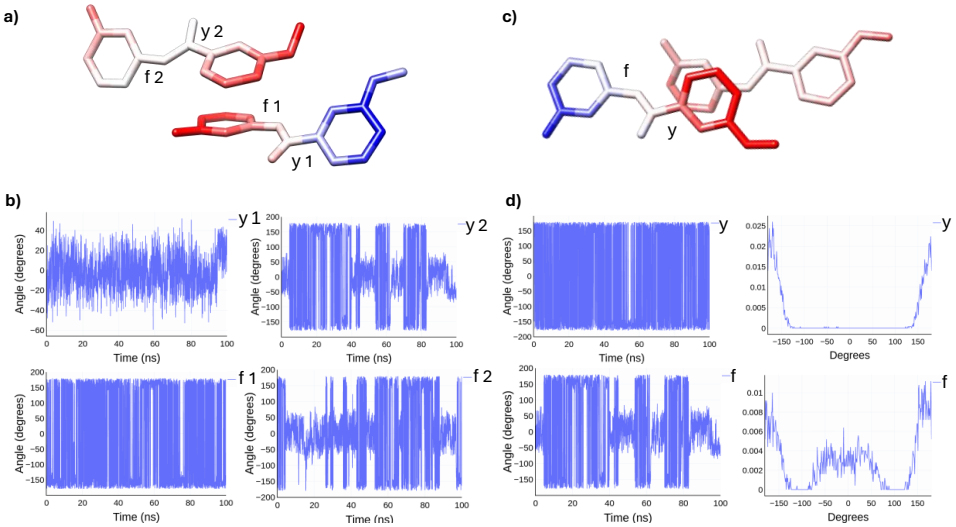


Figure 12. (**a**) The asymmetric unit of polymorph II at the crystal surface, coloured to reflect computed root-mean-square fluctuations (RMSFs) from the lowest (blue) to the highest (red) flexibility. Torsional angles Ψ and ϕ are highlighted for each monomer. (**b**) Sampling over torsional angles Ψ and ϕ of each monomer shown in (**a**) over 100 ns of equilibrium MD simulations. (**c**) The asymmetric unit of polymorph II at the crystal surface after the phase transition resembling polymorph I with molecules coloured as in (**a**). (**d**) Sampling over torsional angles Ψ and ϕ over 100 ns of equilibrium MD simulations and the torsional distribution of Ψ and ϕ angles for the phase-transitioned polymorph II.

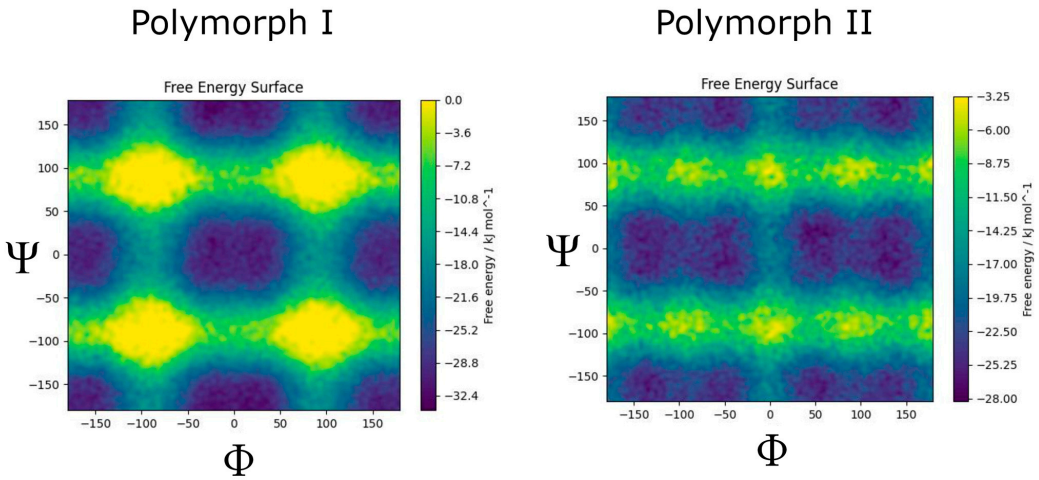


Figure 13. Potential energy surfaces of both polymorphs explored during well-tempered metadynamics simulations. The ϕ (*X*-axis) and Ψ (*Y*-axis) dihedral angles were selected as collective variables. During the simulations, the molecules were biased to explore all possible combinations of ϕ and Ψ dihedrals. Energy values [kJ/mol] are indicated by colour gradient, from dark blue (minima) to yellow (maxima).

4. Conclusions

The crystal structures of polymorphs I and II of *N*-(3-hydroxyphenyl)-3-methoxybenzamide have been determined and compared. The features detailed in this analysis, such as the number of molecules in the asymmetric unit, the dimensionality of the hydrogen

bonding network, and the nature of the intermolecular interactions in the structures, rationalise the differences in crystal habit, density, and melting point between the two forms and demonstrate that aspects of the structure can be correlated with the material properties.

Polymorph I exhibits a hydrogen bonding network in three dimensions, high symmetry ($Z' = 1$) and a lower density. In contrast, the denser polymorph II bears many of the hallmarks of a metastable form; $Z' = 2$, disorder, crystal packing that exhibits approximate symmetry and hydrogen-bonded layers held together by π interactions. The results of the molecular dynamics simulations provide insight into the polymorphic transition of polymorph II to polymorph I that was observed and attests to the metastable nature of polymorph II.

Systematic studies of this kind are important when it comes to understanding polymorphism, which is often hard to predict. This analysis provides insights into the solid-state chemistry of *N*-arylbenzamides specifically, and small organic molecules in general and will prove useful to those in the pharmaceutical, crystallographic and physico-chemical fields.

Supplementary Materials: The following supporting information can be downloaded at https://www.mdpi.com/article/10.3390/cryst14121070/s1. Figure S1: (a) Polymorph I. (b) Polymorph II. Figure S2: ^{1}H NMR Spectrum of *N*-(3-hydroxyphenyl)-3-methoxybenzamide. Figure S3: ^{13}C NMR spectrum of *N*-(3-hydroxyphenyl)-3-methoxybenzamide. Figure S4: COSY NMR spectrum of *N*-(3-hydroxyphenyl)-3-methoxybenzamide. Figure S5: HMBC NMR spectrum of *N*-(3-hydroxyphenyl)-3-methoxybenzamide. Figure S6: HSQC NMR spectrum of *N*-(3-hydroxyphenyl)-3-methoxybenzamide. Figure S7: FTIR spectrum of *N*-(3-hydroxyphenyl)-3-methoxybenzamide. Figure S8: MS spectrum of *N*-(3-hydroxyphenyl)-3-methoxybenzamide.

Author Contributions: Conceptualization, C.C., M.A.C. and P.G.W.; methodology, A.K.B.; software, D.B.; formal analysis, S.K.A.-R., D.B., A.K.B., M.A.C. and P.G.W.; investigation, S.K.A.-R. and M.A.C.; data curation, P.G.W.; writing—original draft preparation, P.G.W.; writing—review and editing, S.K.A.-R., D.B., A.K.B., C.C., M.A.C. and P.G.W.; visualization, P.G.W.; supervision, A.K.B., C.C., M.A.C. All authors have read and agreed to the published version of the manuscript.

Funding: This work was supported by Newcastle University and Fera Science Ltd., through its joint Institute for Agrifood Research Innovation (IAFRI) and the Engineering and Physical Sciences Research Council [Grant number EP/S022791/1].

Data Availability Statement: CCDC 2392575-2392576 contains the full crystallographic data for this article. These are available free of charge at www.ccdc.cam.ac.uk/data_request/cif, by emailing data_request@ccdc.cam.ac.uk or by contacting The Cambridge Crystallographic Data Centre, 12 Union Road, Cambridge, CB2 1EZ, UK; fax: +44 1223 336033. Further synthetic and spectroscopic details are available in the Supplementary Information.

Acknowledgments: PGW would like to thank Carolyn Brock for useful discussions. AKB and DB would like to thank Shangze Xu for discussion of the metadynamics protocol and data visualisation.

Conflicts of Interest: The authors declare no competing financial interests.

References

1. Murakami, K.; Sakamoto, K.; Nishimur, T. Enantioselective C–H alkylation of *N*-arylbenzamides with vinyl ethers catalyzed by an iridium/chiral phosphoramidite–olefin complex. *Synthesis* **2022**, *54*, 4753–4763.
2. Urlam, M.K.; Pireddu, R.; Ge, Y.; Zhang, X.; Sun, Y.; Lawrence, H.R.; Guida, W.C.; Sebti, S.M.; Lawrence, N.J. Development of new *N*-arylbenzamides as STAT3 dimerization inhibitors. *Med. Chem. Commun.* **2013**, *4*, 932–941. [CrossRef] [PubMed]
3. Caldarelli, A.; Minazzi, P.; Canonico, P.L.; Genazzani, A.A.; Giovenzana, G.B. *N*-Arylbenzamides: Extremely simple scaffolds for the development of novel estrogen receptor agonists. *J. Enzym. Inhib. Med. Chem.* **2013**, *28*, 148–152. [CrossRef] [PubMed]
4. Islam, T.; Sarker, M.Z.I.; Uddin, A.B.M.H.; Rashid, S.S.; Bin, L.K. Evaluation of safe mixed solvents in *N*-phenylbenzamide synthesis for alteration of hazardous dipolar aprotic solvents in amide drug syntheses. *Tetrahedron* **2023**, *131*, 1332120. [CrossRef]
5. Urban, B.; Szabo, P.; Sranko, D.; Safran, G.; Kollar, L.; Skoda-Folds, R. Double carbonylation of iodoarenes in the presence of reusable palladium catalysts immobilised on supported phosphonium ionic liquid phases. *Mol. Catal.* **2018**, *445*, 195–205. [CrossRef]

6. Sharma, P.; Jain, N. Chemoselective Synthesis of *N*-arylbenzamides and benzoyloxyacetanilides from aryl isocyanides: Styrene as aryl and arylcarboxymethylene source. *Adv. Synth. Catal.* **2018**, *360*, 1932–1937. [CrossRef]
7. Xu, T.; Alper, H. Pd-Catalyzed Chemoselective Carbonylation of Aminophenols with iodoarenes: Alkoxycarbonylation vs Aminocarbonylation. *J. Am. Chem. Soc.* **2014**, *136*, 16970–16973. [CrossRef]
8. Cruz-Cabeza, A.J.; Feeder, N.; Davey, R.J. Open questions in organic crystal polymorphism. *Commun. Chem.* **2020**, *3*, 142. [CrossRef]
9. Clark, R.C.; Reid, J.S. The analytical calculation of absorption in multifaceted crystals. *Found. Crystallogr.* **1995**, *51*, 887–897. [CrossRef]
10. CrysAlisPro; Rigaku Oxford Diffraction, Tokyo, Japan. Available online: https://rigaku.com/products/crystallography/x-ray-diffraction/crysalispro (accessed on 9 December 2024).
11. Sheldrick, G.M. Crystal structure refinement with SHELXL. *Acta Crystallogr. Sect. C Struct. Chem.* **2015**, *71*, 3–8. [CrossRef]
12. Sheldrick, G.M. A short history of SHELX. *Acta Crystallogr. Sect. A Found. Crystallogr.* **2008**, *64*, 112–122. [CrossRef]
13. Dolomanov, O.V.; Bourhis, L.J.; Gildea, R.J.; Howard, J.A.K.; Puschmann, H. *OLEX2*: A complete structure solution, refinement and analysis program. *J. Appl. Cryst.* **2009**, *42*, 339–341. [CrossRef]
14. Berendsen, H.J.C.; van der Spoel, D.; van Drunen, R. GROMACS: A Message-Passing Parallel Molecular Dynamics Implementation. *Comput. Phys. Commun.* **1995**, *91*, 43–56. [CrossRef]
15. Wang, J.; Wolf, R.M.; Caldwell, J.W.; Kollman, P.A.; Case, D.A. Development and testing of a general Amber force field. *J. Comput. Chem.* **2004**, *25*, 1157–1174. [CrossRef] [PubMed]
16. Lindorff-Larsen, K.; Piana, S.; Palmo, K.; Maragakis, P.; Klepies, J.L.; Dror, R.O.; Shaw, D.E. Improved side-chain torsion potentials for the Amber ff99SB protein force field. *Proteins Struct. Funct. Bioinform.* **2010**, *78*, 1950–1958. [CrossRef]
17. Jakalian, A.; Jack, D.B.; Bayly, C.I. Fast, efficient generation of high-quality atomic charges. AM1-BCC model: II. Parameterization and validation. *J. Comput. Chem.* **2002**, *23*, 1623–1641. [CrossRef] [PubMed]
18. Silva, D.; Vranken, B.F. ACPYPE-AnteChamber PYthon Parser interfacE. *BMC Res. Notes* **2012**, *5*, 367.
19. Jorgensen, W.L.; Chandrasekhar, J.; Madura, J.D.; Impey, R.W.; Klein, M.L. Comparison of simple potential functions for simulating liquid water. *J. Chem. Phys.* **1983**, *79*, 926–935. [CrossRef]
20. Darden, T.; York, D.; Pedersen, L. Particle mesh Ewald: An N·log(N) method for Ewald sums in large systems. *J. Chem. Phys.* **1993**, *98*, 10089–10092. [CrossRef]
21. Bussi, G.; Donadio, D.; Parrinello, M. Canonical sampling through velocity rescaling. *J. Chem. Phys.* **2007**, *126*, 014101. [CrossRef]
22. Hess, B.; Bekker, H.; Berendsen, H.J.C.; Fraaije, J.G.E.M. LINCS: A Linear Constraint Solver for molecular simulations. *J. Comput. Chem.* **1997**, *18*, 1463–1472. [CrossRef]
23. Parrinello, M.; Rahman, A. Polymorphic transitions in single crystals: A new molecular dynamics method. *J. Appl. Phys.* **1981**, *52*, 7182–7190. [CrossRef]
24. Bonomi, M.; Branduardi, D.; Bussi, G.; Camilloni, C.; Provasi, D.; Raiteri, P.; Donadio, D.; Marinelli, F.; Pietrucci, F.; Broglia, R.A.; et al. PLUMED: A portable plugin for free-energy calculations with molecular dynamics. *Comput. Phys. Commun.* **2009**, *180*, 1961–1972. [CrossRef]
25. d'Agostino, S.; Braga, D.; Grepioni, F.; Taddei, P. Intriguing Case of *Pseudo*-Isomorphism between Chiral and Racemic Crystals of rac-and (*S*)/(R)2-(1,8-Naphthalimido)-2-quinuclidin-3-yl, and Their Reactivity Toward I_2 and Br_2. *Cryst. Growth Des.* **2014**, *14*, 821–829. [CrossRef]
26. Potter, Z.E.; Hill, M.; Sellars, J.D.; Waddell, P.G. A New Polymorph of *tert*-Butyl (2-Aminophenyl)Carbamate. *J. Chem. Cryst.* **2024**, *54*, 285–290. [CrossRef]
27. Etter, M.C. Encoding and Decoding Hydrogen-Bond Patterns of Organic Compounds. *Acc. Chem. Res.* **1990**, *23*, 121–126. [CrossRef]
28. Brock, C.P. High-Z′ structures of organic molecules: Their diversity and organizing principles. *Acta Crystallogr. Sect. B Struct. Sci. Cryst. Eng. Mater.* **2016**, *72*, 807–821. [CrossRef]
29. Brock, C.P. Pseudosymmetric layers in high-*Z*′ and *P*1 structures of organic molecules. *CrystEngComm* **2020**, *22*, 7371–7379. [CrossRef]
30. Brock, C.P. Pervasive approximate periodic symmetry in organic *P*1 structures. *Acta Crystallogr. Sect. B Struct. Sci. Cryst. Eng. Mater.* **2022**, *78*, 576–588. [CrossRef]
31. Avasthi, K.; Shukla, L.; Kant, R.; Pavikumar, K. Folded conformations due to arene interactions in dissymmetric and symmetric butylidene-linker models based on pyrazolo[3,4-*d*]pyrimidine, purine and 7-deazapurine. *Acta Crystallogr. Sect. C Struct. Chem.* **2014**, *70*, 555–561. [CrossRef]
32. Steed, K.M.; Steed, J.W. Packing Problems: High Z′ Crystal Structures and Their Relationship to Cocrystals, Inclusion Compounds, and Polymorphism. *Chem. Rev.* **2015**, *115*, 2895–2933. [CrossRef] [PubMed]

Disclaimer/Publisher's Note: The statements, opinions and data contained in all publications are solely those of the individual author(s) and contributor(s) and not of MDPI and/or the editor(s). MDPI and/or the editor(s) disclaim responsibility for any injury to people or property resulting from any ideas, methods, instructions or products referred to in the content.